LIMNOLOGY and OCEANOGRAPHY

ASLO

Limnol. Oceanogr. 9999, 2024, 1–14

doi: 10.1002/lno.12557

Decadal changes in surface CO_2 concentrations and CO_2 fluxes in a mountain lake

Ulrike Obertegger,[1*] **Stefano Corradini**,[2] **Leonardo Cerasino**,[1] **Linda C. Weiss**[3]

[1]Fondazione Edmund Mach, Research and Innovation Centre, Hydrobiology Research Unit, San Michele all'Adige, Italy
[2]Fondazione Edmund Mach, Technology Transfer Centre, Agrometeorology and Informatics Unit, San Michele all'Adige, Italy
[3]Department of Animal Ecology, Evolution and Biodiversity, Ruhr-University Bochum, Bochum, Germany

Abstract

Climate warming impacts biogeochemical cycles in lakes. However, the factors controlling CO_2 dynamics in mountain lakes over multidecadal scales are poorly understood. Here, we capitalized on long-term monthly data (1995–2022) of oligotrophic mountain Lake Tovel and calculated surface CO_2 concentrations and flux by applying geochemical relationships and the thin boundary layer approach. Advanced time-series and regression modeling was used to determine temporal patterns and environmental parameters explaining surface CO_2 concentrations and flux. Surface CO_2 concentrations were highest from 2009 to 2017 (annual mean: 109.1 μmol CO_2 L^{-1}) but lower before and after this period. Concomitantly, the air–water CO_2 flux (μmol CO_2 m^{-2} d^{-1}) showed a period of lowest ($mean_{1995–2010}$: 6.4 ± 0.7), highest ($mean_{2011–2017}$: 35.7 ± 2.1), and intermediate emissions ($mean_{2018–2022}$: 19.3 ± 4.7). Temporal modeling showed that hypolimnetic and deep hypolimnetic dissolved oxygen (DO) had the same change points and trends as surface CO_2 concentrations. In multiple linear regression, hypolimnetic DO, silica, and the standardized precipitation index (pseudo-$R^2_{adj.} = 0.62$; $p < 0.01$) best predicted annual mean surface CO_2 concentrations. Regression results and the overlap between temporal trend patterns indicated that surface CO_2 concentrations of Lake Tovel were positively influenced by external (loading of allochthonous carbon) and internal (lake autumn mixing) factors. The recent decline in surface CO_2 concentrations from the year 2018 was attributed to increased stratification that offset lake autumn mixing and thus lead to the observed decline. These results help us to better understand the carbon cycle in mountain lakes in a changing climate.

Carbon dioxide (CO_2) air–water emissions from lakes are an important component of the global carbon cycle and are inherently linked to surface CO_2 concentrations. Surface CO_2 concentrations are influenced by a complex interaction of biochemical (photosynthesis and respiration), chemical (carbonate dissolution and precipitation, photooxidation of organic matter), physical (temperature), and hydrological (allochthonous carbon input and mixing) factors (Vachon et al. 2020). For example, the input of allochthonous carbon by groundwater (Striegl and Michmerhuizen 1998) or by storm related precipitation (Vachon and Del Giorgio 2014) increase surface CO_2. Surface CO_2 can further increase through intensified mixing bringing hypolimnetic CO_2 to the surface (Baltic Sea: Kuss et al. 2006; Mediterranean reservoirs: Morales-Pineda et al. 2014) and by CO_2-producing calcite precipitation during photosynthesis (Escoffier et al. 2023).

Air–water CO_2 emissions depend on physical processes such as wind stress, convection, and currents. The gas transfer velocity (k_{CO2}) describes the efficiency of transfer across the water–air interface. Changes in k_{CO2} are primarily driven by diel and seasonal variations in mass and energy fluxes at the lake surface (Dugan et al. 2016). While at best k_{CO2} should be measured, it can also be modeled introducing uncertainty into estimates of CO_2 emissions (Dugan et al. 2016). Since over long time scales (days to weeks), the variability in surface CO_2 concentrations is greater than that of k_{CO2} and affects CO_2 fluxes more than k_{CO2} (Natchimuthu et al. 2017), monthly long-term studies based on modeled k_{CO2} can adequately capture CO_2 emissions.

Climate change generally impacts biogeochemical cycles in lakes (Moss 2012). Contrary to low-land lakes, mountain lakes

*Correspondence: ulrike.obertegger@fmach.it

Additional Supporting Information may be found in the online version of this article.

Author Contribution Statement: U.O. involved in conceptualization, writing, and formal analysis. L.C.W. performed in formal analysis and writing. S.C. performed data curation. L.C. performed data curation. All authors contributed to subsequent versions of the manuscript.

are highly sensitive to on-going climate warming (Thompson et al. 2005). Mountain lakes are characterized by cold temperatures, high incident solar radiation, prolonged ice and snow cover, and low nutrient content (Moser et al. 2019). With climate change, mountain lakes will likely have significant changes. In mountain lakes, for example, lake stratification is stronger because of a shift from a nival to pluvial recharge of the aquifer (Flaim et al. 2019), lake CO_2 efflux is higher driven by large flushing events (Ejarque et al. 2021), and epilimnetic summer temperatures are higher because of a shorter duration of ice cover and reduced amount of snowmelt water (Sadro et al. 2019). A reduced ice-cover leads to a shorter period of under-ice respiration of organic matter (Baehr and DeGrandpre 2002), and thus reduced CO_2 accumulation under ice (Finlay et al. 2015). Most studies on carbon cycling in mountain lakes rely on annual analyses (Seekell and Gudasz 2016; Ejarque et al. 2021; Scholz et al. 2021) or spot sampling (Pighini et al. 2018) while little is known about CO_2 patterns over decades (but see Saidi and Koschorreck 2017; Escoffier et al. 2023). Considering the scarcity of long-term data, the CO_2 dynamics and its driving factors in mountain lakes remain poorly understood (Ejarque et al. 2021; Scholz et al. 2021).

This study investigates the temporal patterns of surface CO_2 concentrations and CO_2 fluxes and their driving forces in Lake Tovel, an oligotrophic mountain lake. Lake Tovel shifted from meromixis to dimixis that led to hypolimnetic oxygenation (Flaim et al. 2020) but with unknown consequences for CO_2 dynamics. Changing hypolimnetic oxygen substantially influences lake biochemical processes such as sediment fluxes of carbon, nitrogen, and phosphorus (higher flux with anoxic conditions; Carey et al. 2022), and these changes in turn may impact CO_2 dynamics. This study builds on Flaim et al. (2020) and investigates drivers of surface CO_2 concentrations and the inter-relationships between surface CO_2 concentrations, CO_2 emissions, and hypolimnetic dissolved oxygen (DO). We hypothesize (1) that surface CO_2 and CO_2 fluxes mirror DO changes under the condition of the same driving forces (i.e., changes in mixing patterns); and (2) that CO_2 fluxes are low considering Lake Tovel's oligotrophic state.

Material and methods

Study site

Lake Tovel (46.26137°N, 10.94934°E; 1177 m above sea level [asl]; area: 0.4 km^2; maximum depth: 39 m) is an Italian long-term ecological research site (LTER_EU_IT_090) in the Brenta Dolomites and belongs to international networks (LTER-Europe and ILTER). Lake Tovel is usually frozen from late December to mid-April with a mean ice thickness of 35 cm (range: 17–65 cm; $n = 14$; 2002–2023) and has low wind speeds (< 0.7 m s^{-1}; Flaim et al. 2020). The lake is oligotrophic (mean annual values for the whole water column: total dissolved phosphorus < 10 $\mu g\ L^{-1}$, dissolved organic carbon < 1 mg L^{-1}, conductivity ~ 180 $\mu S\ cm^{-1}$; coefficient of light attenuation ≤ 0.18, and water transparency > 10 m; depth layer 0–20 m: chlorophyll *a* (Chl *a*) < 3 $\mu g\ L^{-1}$; Cellamare et al. 2016). According to $CaCO_3$ ranges (83–155 mg $CaCO_3\ L^{-1}$ over the whole water column from 1995 to 2022), Lake Tovel is a moderately hard to hard water lake according to the United States Geological Survey (2023). Surface HCO_3^- ranged from 106 to 146 mg L^{-1} between 1995 and 2022 (Supporting Information Fig. S1B), and surface pH ranged from 7.63 to 8.65 (Supporting Information Fig. S1B). At these observed pH values, most of the inorganic carbon was found as HCO_3^-.

Sampling

Since 1995, sampling is monthly over the deepest part of the lake during the ice-free period (May to November), with restricted site access during winter (December to April). Vertical profiles of water temperature and DO were taken with a multiparametric probe (Hydrolab Surveyor from 1995 to 2010 and Idronaut Ocean 316 from 2011 onwards) between 10:00 h and 11:00 h. Water samples for nutrients (nitrate, ammonium, total phosphorus (P_{tot}), silica, pH, and hydrogen carbonate) and other chemical parameters (ions) were taken with a bottle at 5-m intervals and were analyzed as described in Cellamare et al. (2016). Zooplankton samples were taken by vertical tows (mesh size = 50 μm) from the bottom to the surface. Zooplankton composition and biomass were determined as described in Obertegger et al. (2007). Water samples for Chl *a* were taken with a 20-m long tube (weighted at the bottom), and Chl *a* was extracted (Whatman GF/C and GF/F filters) from 1 L with 90% acetone and determined spectroscopically according to the trichromatic method (Rice et al. 2017).

Meteorological indices

Precipitation, air temperature, and wind velocity were provided by the on-site station (Metex system until 2010, afterwards Nesa system; one-hour recording frequency). Missing daily data (1995–2022: 24% to 34% missing; Supporting Information Table S1) were imputed applying boosted regression trees (library caret; Kuhn 2022) based on data from a close by station (46.361°N, 11.040°E; 656 m asl; 13 km from Lake Tovel). The standardized precipitation index (SPI; reference period: 1995 to 2010; library standardized; Maetens 2019) was calculated to characterize monthly precipitation.

Water column stability

We assessed the temporal patterns of monthly and annual mean surface water temperature, SPI, and Schmidt stability. Schmidt stability was calculated based on probe temperature profiles as an index for the energy required to mix the water column to uniform density (library rLakeAnalyzer; Winslow et al. 2019). Furthermore, we calculated the duration of deep spring and autumn mixing, respectively, as the number of days when the mixing depth was greater than or the same as 30 m after ice-out and in autumn, respectively. The autumn

deep mixing period was estimated as the number of days between onset of deep autumn mixing and ice-in. Mixing depth was determined according to Wilson et al. (2020) using daily mean water temperature provided by sensors from 2010 to 2022 (Supporting Information Data S1). Ice-in dates (period 1995–2019) were taken from Flaim et al. (2020) determining ice-in as the day of the year when mean daily air temperature was < 0°C for at least four consecutive days and mean daily surface water temperature was < 4°C. Ice-in for the period 2020–2022 were determined based on webcam images.

pCO_2 calculations

In the absence of measurements, we calculated pCO_2 based on geochemical relationships (library tidyphreeqc; Parkhurst and Appelo 2013) as done in other studies (e.g., Seekell and Gudasz 2016; Wiik et al. 2018; Toavs et al. 2023). Geochemical relationships approximate measurements well with circumneutral to basic pH and with total alkalinity exceeding 1000 μmol L^{-1} (Abril et al. 2015; our study site: mean ± one standard deviation $pH_{1995–2022} = 8.1 \pm 0.25$; total $alkalinity_{1995–2022} = 1040 \pm 74$ μmol L^{-1}). pCO_2 (atm) was converted to CO_2 concentrations (μmol L^{-1}). Only surface (0 m; $n = 239$), hypolimnetic (30–35 m; $n = 234$), and deep hypolimnetic CO_2 concentrations (> 35 m; $n = 193$; some samplings were missing because the lake did not always have depths > 35 m) with an ion-balance error < 15% were considered (Supporting Information Data S2). The period considered here spans May 1995 to February 2023 in contrast to Flaim et al. (2020) considering pre-1995 samplings that lack data for pCO_2 calculations.

To investigate a potential link between water temperature and hypolimnetic CO_2 production, we analyzed the temporal pattern of monthly and annual hypolimnetic temperature (mean from 30 to 35 m depth).

Atmospheric CO_2 flux

The atmospheric CO_2 flux (F_{CO2}; mol CO_2 m^{-2} d^{-1}; $n = 239$) across the air to water interface was calculated using Fick's law of gas diffusion: $F_{CO2} = \alpha$ * k_{CO2} * Kh * ($pCO_{2\ water} - pCO_{2\ air}$). α is the ratio between the enhanced and the nonenhanced gas transfer velocity (Kuss and Schneider 2004), Kh is the Henry's coefficient corrected for temperature, and pCO_2 (atm) is the CO_2 partial pressure at the water surface ($pCO_{2\ water}$) and in the atmosphere ($pCO_{2\ air}$). For atmospheric pCO_2, we used midday data of the atmospheric mixing ratio of CO_2 (ppm) from a public German monitoring station (Schauinsland, Germany, 1204 m a.s.l; Supporting Information Data S3), that is at an altitude and in a coniferous forest like Lake Tovel. We acknowledge that atmospheric CO_2 values from a German weather station might not adequately reflect local short-term conditions to calculate CO_2 flux and mainly focused on large-scale temporal patterns. The gas exchange coefficient k_{CO2} was determined from k_{600}, standardized to a Schmidt number of 600 using the following equation: $k_{CO2} = k_{600}$ * $(Sc_{CO2}/600)^{-n}$ where Sc_{CO2} is the CO_2 Schmidt number for a given temperature and n is − 2/3 with a wind speed < 3 m s^{-1} or is − 0.5 with a speed > 3 m s^{-1} (Bade 2009). We used a surface renewal model (Read et al. 2012) as provided in library LakeMetabolizer (function k.read.soloviev.base; Winslow et al. 2016) to calculate k_{600}. The CO_2 flux for the ice cover period was set to zero. We calculated the average carbon emission of Lake Tovel for the ice-free period considering its surface area and mean annual CO_2 flux. Thus, several factors such as seasonal effects or potentially different emission from littoral lake areas were not included.

Upper layer, hypolimnetic, and deep hypolimnetic DO

All mg DO L^{-1} values of the multiparametric probe were converted to percent DO saturation (% DO; library rMR; Moulton 2018) to account for temperature-dependent solubility differences. Upper layer DO, the DO that replenishes oxygen in the hypolimnion, was calculated as % DO from the surface to the first 5 m irrespective of mixing depth. Hypolimnetic DO was calculated as the mean % DO from 30 to 35 m and deep hypolimnetic DO as the mean % DO deeper than 35 m according to Flaim et al. (2020).

Statistical analyses

All calculations, data management, and statistical analyses were done using R 4.3.0 (R Core Team 2023). In all models, R^2 adjusted values ($R^2_{adj.}$; Supporting Information Data S3) were reported as a measure of fit adjusted for the number of used predictors.

Seasonal differences

Differences between seasons in surface CO_2 concentrations, k_{CO2}, and CO_2 flux were investigated by generalized mixed modeling with library lme4 (Bates et al. 2015) using year as random intercept and a Gamma and Normal distribution where appropriate. Post-hoc testing corrected for multiple testing was performed (library emmeans; Lenth 2022).

Temporal modeling of monthly data

Seasonality and trend (i.e., the long-term change in the level of the time-series) were modeled using generalized additive modeling (GAM) and generalized additive mixed modeling (GAMM) considering temporal dependence by including an autocorrelation term nested within years. Importantly, GAM accounts for nonlinearity and does not rely on subjective model specification. For the seasonal term, we used a cyclical cubic spline determining continuity between the first and last seasonal observations. We calculated the first derivative of smoothing splines (library gratia; Simpson 2023) to determine significant periods of increase and decrease in the seasonal and long-term pattern, respectively. We used a Gamma distribution, appropriate for only positive data, for seasonal DO and CO_2 data and Schmidt stability, while a

normal distribution for SPI, surface and hypolimnetic water temperature, and CO_2 flux.

Annual trends

Annual trends of the day of the year of ice-in and mixing depth were modeled using a quasi-Poisson distribution to account for count-data and their large variance. For annual mean data, we only considered values from April to November to focus on the ice-free period. We applied a shift in the mean analysis (see Flaim et al. 2020) and a piece-wise regression model (a.k.a. segmented regression; library segmented; Muggeo 2017). Goodness of fit of the shift in the mean analysis vs. a piece-wise regression model was investigated by the root mean square error (RMSE) with the model having the lowest value preferred. We used a Gamma distribution for annual mean data of DO, CO_2 concentrations, and Schmidt stability, while a normal distribution for SPI, surface and hypolimnetic water temperature, and CO_2 flux. Where appropriate, we reported pseudo-$R^2_{adj.}$ values (library rcompanion; Mangiafico 2017) because non-linear regression models (e.g., quasi-Poisson, Gamma regression) do not use the ordinary least squares estimation technique to fit the model.

Environmental modeling of surface CO_2 concentrations

Monthly surface CO_2 of the ice-free period (April to November; $n = 177$) was modeled dependent on environmental variables (ammonium, nitrate, P_{tot}, calcium, and silica as average from the surface to 35 m, crustacean, rotifer, and zooplankton biomass, Chl *a*, Schmidt stability, hypolimnetic DO and meteorological variables). As meteorological variables, SPI and the sum of precipitation, average minimal and mean air temperature and average mean and maximum wind speed over 30, 20, 10, 5, 2, and 1 d before the sampling to account for any lag-effect of meteorological events influencing mixing as shown by Flaim et al. (2020). We used a partial least squares (PLS) model that can handle collinear predictors (mainly meteorological predictors) from library tidymodel (Kuhn and Wickham 2020) to select the most important variables based on the inflection of the importance score (Supporting Information Data S4). These predictors were used in generalized linear regression accounting for temporal dependence by an autocorrelation term. In regression, predictors were standardized to compare regression coefficients, and model residuals were inspected for model fit (mainly autocorrelation and heterogeneity of residuals).

Annual mean surface CO_2 of the ice-free period ($n = 28$) was modeled dependent on the same predictors as used in monthly modeling. For variable selection, we used PLS (no splitting in train and test data because of the reduced dataset) and variable ranking. Variable ranking is based on mutual information (library varrank; Kratzer and Furrer 2022) and compares the relevancy to redundancy balance of information across the set of variables. Based on the inflection of the scores, the most important variables were selected in variable ranking and PLS. In variable ranking of average annual meteorological predictors, the annual average of the mean wind over 2 d before sampling, the annual average of minimum temperature over 5 d before sampling, and the annual average of the total sum of rain over 30 d before sampling were selected. After variable selection, generalized linear regression, accounting for temporal dependence by an autocorrelation term, was used. In regression, predictors were standardized to compare regression coefficients, and model residuals were inspected for model fit (mainly autocorrelation and heterogeneity of residuals).

Link between climate-induced mixing indices and surface CO_2 concentrations and CO_2 flux

We used the correlation between ice-in day of the year (doy; proxy for autumn mixing), hypolimnetic DO (proxy for deep-water column mixing), Schmidt stability (index of water column mixing) and surface CO_2 concentrations and CO_2 flux to infer any potential link. Ice-in doy was used as it is and also backshifted for 1 yr (lagged ice-in) to investigate the correlation between ice-in of the preceding year on parameters of the following year.

Results

Water column stability

In GAMM ($R^2_{adj} = 0.86$; $p < 0.01$; Supporting Information Table S2), monthly surface water temperature showed a continuously increasing trend ($+ 0.5°C$ decade^{-1}; Supporting Information Fig. S2A) and a seasonal pattern (highest temperature during summer, lowest temperature during winter; Supporting Information Fig. S2B). Annual mean surface water temperature ($mean_{1995–2022}$: $12.2 \pm 0.8°C$) did not show any temporal pattern (no change point, no continuous regression, nor a piece-wise regression). Monthly and annual mean values of SPI ($mean_{1995–2022}$: 0.05 ± 0.98) as a proxy for precipitation did not show a temporal pattern (Supporting Information Fig. S2C,D).

The onset of deep spring mixing (2010–2022) occurred during mid- to late-April. Spring mixing, its onset or length did not have a temporal pattern. On average, deep spring mixing lasted 2 d; only in 2014, deep mixing lasted 5 d. Also, the onset of deep autumn mixing (2009–2022) and its duration did not show a temporal pattern. On average, deep autumn mixing started in mid-November and lasted 30 d ($\pm$ 9 d); only in 2010, deep mixing lasted 51 d (Supporting Information Fig. S3).

Ice-in occurred later from 1995 to 2022 (quasi-Poisson regression; pseudo-$R^2_{adj.} = 0.33$; $p < 0.001$; Fig. 1; Supporting Information Table S3). Ice-in occurred on average 14 d later in 2022 compared with 1995. Especially, ice-in in 2022 occurred late with several episodes of ice-in and ice-out during December 2022 and a permanent ice cover only after mid-January 2023 (Fig. 1).

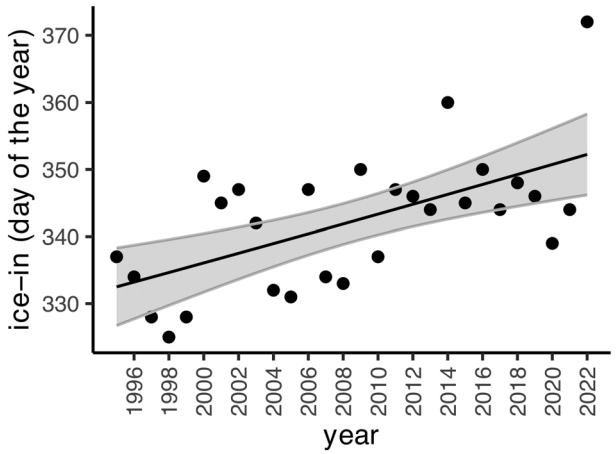

Fig. 1. Linear regression of ice-in day of the year dependent on year (quasi-Poisson regression; pseudo-$R^2_{adj.} = 0.33$; $p < 0.001$); the gray band indicates the 95% confidence interval for the trend; day of the year exceeds 365 d to account for the late ice in of winter 2022 in January 2023.

In GAMM with monthly Schmidt stability (1995–2022), Gamma distribution did not converge and therefore a normal distribution was used. Residuals of this model were well approximated by a normal distribution justifying its use. Monthly Schmidt stability only showed a seasonal pattern ($R^2_{adj.} = 0.61$, $p < 0.001$; Supporting Information Table S4; Fig. S4A) increasing from May to mid-August and decreasing from mid-August to mid-November (Supporting Information Fig. S4B). Annual mean Schmidt stability ($R^2_{adj.} = 0.23$, $p < 0.05$; Supporting Information Table S5; Fig. S4C) showed an increase until 2003 (13.8 J m^{-2} yr^{-1}) and then a slight decrease (– 7 J m^{-2} yr^{-1}).

Surface, hypolimnetic, and deep hypolimnetic CO_2 concentrations

Monthly data

The lowest surface CO_2 was observed in August 1995 (10 μmol L^{-1}) and the highest under ice in 2018 (452 μmol L^{-1}; Fig. 2a). Comparing seasons (Fig. 2a), mean surface CO_2 was lowest during summer ($p < 0.001$; range: 10–217 μmol L^{-1}; mean: 44.6 μmol L^{-1}) and was highest under ice ($p < 0.001$; range: 54.3–452 μmol L^{-1}; mean: 133 μmol L^{-1}) than during other seasons. Mean spring (range: 25.2–236 μmol L^{-1}; mean: 69 μmol L^{-1}) and autumn surface CO_2 (range: 17.3–232 μmol L^{-1}; mean: 71 μmol L^{-1}) were not different ($p > 0.05$).

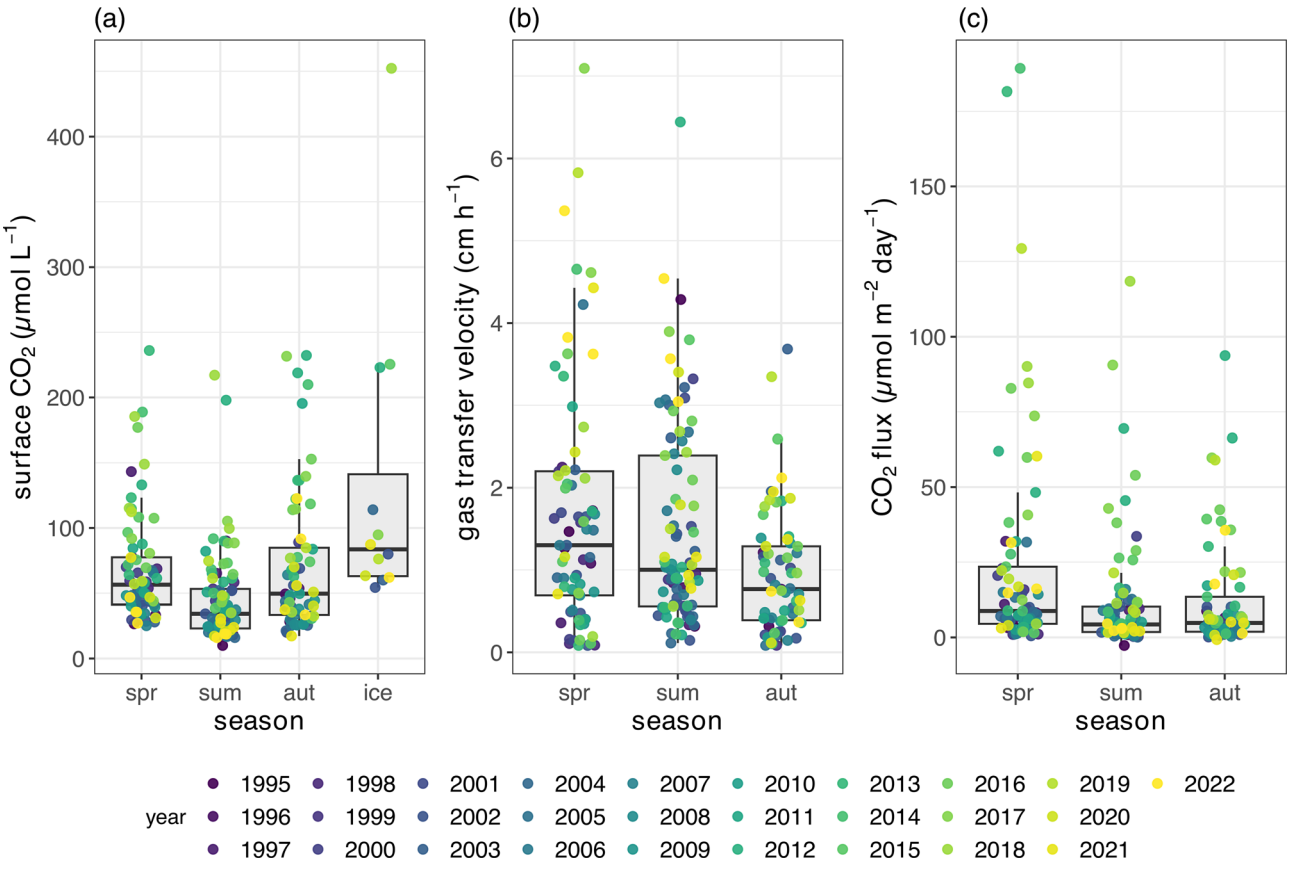

Fig. 2. Boxplots of observed (**a**) surface CO_2, (**b**) gas transfer velocity, and (**c**) CO_2 flux split by seasons (spring—spr; summer—sum; autumn—aut; under ice—ice).

In GAMM, monthly surface CO_2 showed a trend and a seasonal pattern (Table 1; Fig. 3a; Supporting Information Table S6). The trend showed a statistically significant increase with the year 1995 and the year 2009 and a decrease with the year 2018 (Table 1). The seasonal pattern showed an increase from September to January and a decrease from mid-February to mid-March and from end of May to July (Supporting Information Fig. S5A).

Monthly hypolimnetic (range: 1017–12,470 μmol L^{-1}) and deep hypolimnetic CO_2 (range: 628–16,303 μmol L^{-1}) were higher than monthly surface CO_2 (range: 10–452 μmol L^{-1}). Monthly hypolimnetic and deep hypolimnetic CO_2 values were correlated ($r_{Pearson} = 0.89$, $p < 0.001$), and their trends showed similar periods of decrease and increase (Table 1; Fig. 3c,d; Supporting Information Table S6). The hypolimnetic and deep hypolimnetic CO_2 decreasing trend around 1996 (even though their temporal durations were quite short), the decreasing trend around 2018 and the increasing trend around 2010 were also observed in the trend of monthly surface CO_2 (Table 1; Fig. 3a,-c,d). In contrast, the decreasing trends of hypolimnetic and deep hypolimnetic CO_2 with the years 2000 and 2012 were not observed in surface CO_2 (Table 1; Fig. 3a,c,d), implying that hypolimnetic and surface CO_2 were not strictly linked.

Monthly hypolimnetic water temperature only showed a weak seasonal pattern with highest values during September to November ($R^2_{adj.} = 0.17$, $p < 0.001$; Supporting Information Fig. S6A).

Annual mean data

With the shift in the mean analysis for annual mean surface CO_2, two change points were found while piece-wise regression analysis was not significant (Table 2; Fig. 4a). In detail, the periods 1995–2008 ($mean_{1995–2008}$: 42 ± 15.8 μmol CO_2 L^{-1}) and 2018–2022 ($mean_{2018–2022}$: 58 ± 37.0 μmol CO_2 L^{-1}) showed similar CO_2 ($p > 0.05$), and the intermediate period 2009–2017 ($mean_{2009–2017}$: 78 ± 26.7 μmol CO_2 L^{-1}; Fig. 4a) showed higher CO_2 ($p < 0.001$) than the periods before and after (Fig. 4a).

Annual mean hypolimnetic and deep hypolimnetic CO_2 were quite similar ($r_{Pearson} = 0.97$; $p > 0.001$), both did not show any temporal pattern and did not mirror annual mean surface CO_2 (Table 2; Fig. 4c,d).

Yearly mean hypolimnetic water temperature did not show any temporal pattern ($mean_{1995–2022} = 4.9 \pm 0.2$°C; Supporting Information Fig. S6B).

CO_2 flux

Seasonal differences, monthly, and annual mean data

CO_2 flux depends on surface CO_2 and the gas transfer velocity (k_{CO2}). Here, k_{CO2} was higher ($p < 0.001$) during spring (range k_{CO2}: 0.08–7.1 cm h^{-1}; 0.02–1.7 m d^{-1}) and summer (range k_{CO2}: 0.1–6.4 cm h^{-1}; 0.02–1.5 m d^{-1}) than autumn (range k_{CO2}: 0.08–3.7 cm h^{-1}; 0.02–0.8 m d^{-1}; Fig. 2b) with no difference between summer and autumn ($p > 0.05$; Fig. 3c). Similarly, the CO_2 flux was higher during spring (range: 0.5–189.2 μmol CO_2 m^{-2} d^{-1}) than during summer (range: −2.7–118.5 μmol CO_2 μmol m^{-2} d^{-1}; $p < 0.01$) and autumn (range: −0.7–93.7 μmol CO_2 m^{-2} d^{-1}; $p < 0.05$) with no difference between summer and autumn ($p > 0.05$; Fig. 2c).

In GAM, the monthly CO_2 flux showed a trend and a seasonal pattern. The trend showed an increase from November 2010 to September 2012 and a decrease from December 2018 to

Table 1. Results of GAMM of CO_2 and DO; for the trend, the periods of statistically significant increases and decreases are reported; R^2 adjusted (R^2 adj.); hypolimnetic (hypo.); * indicates that the pattern was modeled by GAM.

		Trend		
Parameter	R^2 adj. Significance	Increase	Decrease	Monthly pattern
Surface CO_2	0.52	May 1995–Aug 1997	Jan 2018–May 2021	Yes
	$p < 0.001$	June 2009–Sept 2012		
Hypo. CO_2	0.42	June–Aug 1996	Oct 1999–April 2002	No
	$p < 0.001$	June 2009–April 2011	Aug 2012–Nov 2013	
		Dec 2020–Feb 2023	Sept 2017–Dec 2018	
Deep hypo. CO_2	0.49	June–Sept 1996	June 2000–July 2002	No
	$p < 0.001$	May 2009–April 2011	Dec 2011–Nov 2013	
		Oct 2020–Dec 2020	Aug 2017–Aug 2018	
CO_2 flux*	0.29	Nov 2010–Sept 2012	Dec 2018–Aug 2020	Yes
	$p < 0.001$			
Upper layer DO	0.45	No	No	Yes
	$p < 0.001$			
Hypo. DO	0.53	Aug 2000–Feb 2002	Dec 2018–Oct 2021	Yes
	$p < 0.001$	April 2009–Dec 2011		
Deep hypo. DO	0.47	May 2009–July 2012	Aug 2019–Dec 2022	No
	$p < 0.001$			

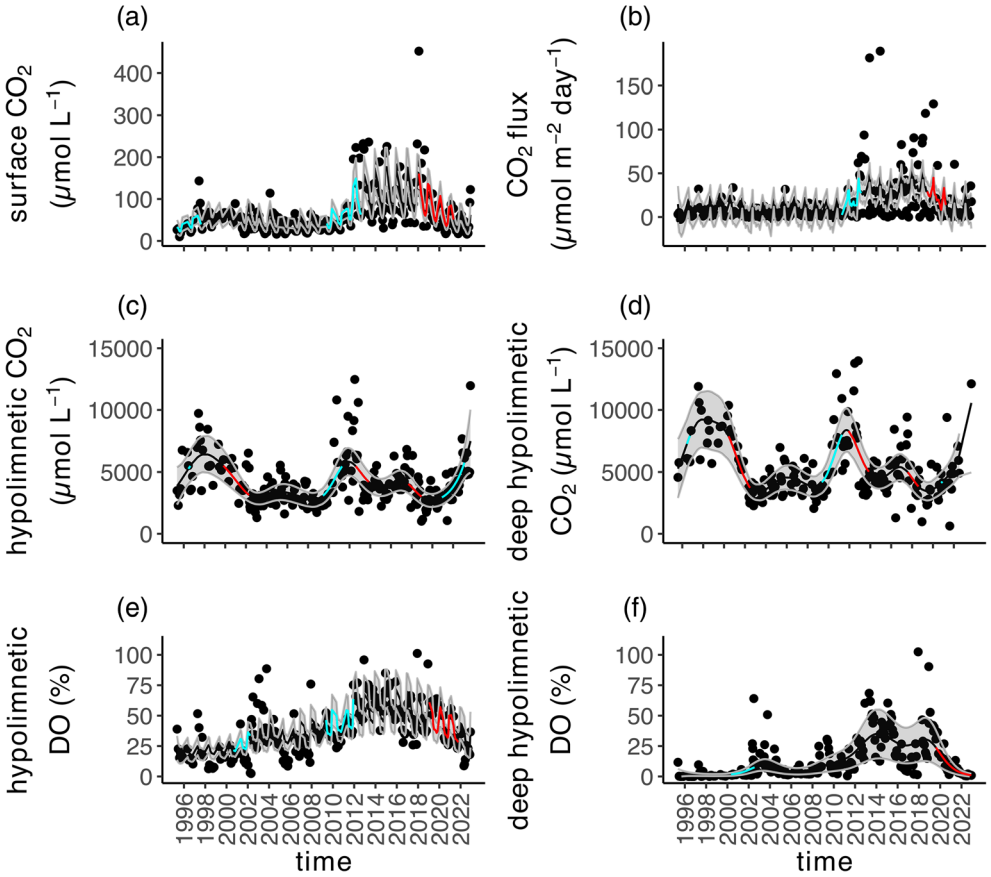

Fig. 3. Monthly observed values (black points) and modeled temporal patterns (continuous black line) by GAMM with its 95% confidence interval (gray band) for (**a**) surface CO_2 (μmol L^{-1}), (**b**) CO_2 flux (μmol CO_2 m^{-2} d^{-1}), (**c**) hypolimnetic CO_2 (μmol L^{-1}), (**d**) deep hypolimnetic CO_2 (μmol L^{-1}), (**e**) hypolimnetic DO (% saturation), and (**f**) deep hypolimnetic DO (% saturation). Cyan indicates a significant increasing and red a significant decreasing trend.

August 2020 (Table 1; Fig. 3b). The seasonal pattern showed an increase from end of March to mid-April and a decrease from May to June (Supporting Information Fig. S5B). Concomitantly to the trend of monthly CO_2 flux, the annual mean flux showed two change points (Table 2; Fig. 4b) discriminating three periods of lowest ($mean_{1995–2010}$: 6.4 ± 0.7 μmol CO_2 m^{-2} d^{-1}), highest ($mean_{2011–2017}$: 35.7 ± 2.1 μmol CO_2 m^{-2} d^{-1}), and intermediate flux ($mean_{2018–2022}$: 19.3 ± 4.7 μmol CO_2 m^{-2} d^{-1}).

Considering the total lake surface area emitting CO_2 and an average ice-free duration (period between 1 May and ice-in) of 217, 227, and 229 d for these three periods, respectively, the annual mean CO_2 emission was 553 mol CO_2 yr^{-1} for the period 1995–2010, 3240 mol CO_2 yr^{-1} for the period 2011–2017, and 1765 mol CO_2 yr^{-1} for the period 2018–2022 (Supporting Information Table S7).

Environmental modeling of surface CO_2 concentrations for the ice-free period

Monthly data

In PLS regression of monthly surface CO_2 (four PLS components; $R^2_{adj.} = 0.27$), hypolimnetic DO, SPI, sum of rain over 30 d before sampling, P_{tot}, and silica were the most important variables (decreasing order of importance). Using these five variables in multiple linear regression ($R^2_{adj.} = 0.16$; $p < 0.001$), only SPI was not statistically significant. All parameters in the regression increased monthly CO_2 (Supporting Information Fig. S7), and the standardized regression coefficient of hypolimnetic DO (14) was much higher than those of rain (8.4), silica (8.1), and P_{tot} (7.3).

Annual mean data

In variable selection of annual mean environmental data for the modeling of annual mean surface CO_2, variable ranking and PLS indicated almost the same variables as important (Supporting Information Data S5). We used those variables selected by both methods (silica, hypolimnetic DO, P_{tot}, SPI, and yearly mean wind over 2 d before the sampling). In multiple linear regression, hypolimnetic DO, silica, and SPI were statistically significant (pseudo-$R^2_{adj.} = 0.62$; $p < 0.01$; Fig. 5; Supporting Information Table S8), and all variables increased annual mean surface CO_2. Annual mean surface CO_2 was predicted to increase with increasing annual mean hypolimnetic DO and a wetter year (positive SPI; Fig. 5a) and an increasing annual mean silica (Fig. 5b), respectively.

Table 2. Temporal modeling results of the annual mean CO_2 flux, of annual mean surface, hypolimnetic, and deep hypolimnetic (deep hypo.) CO_2 (μmol L^{-1}) concentrations and DO (% saturation), respectively; for the shift in the mean analysis, the 95% confidence intervals for the change point (CP) are given in brackets. For model comparison, the root mean square error (RMSE; the lower, the better) is given; piece-wise regression (piece-wise regr.); not significant (n.s.); per decade (dec^{-1}).

Parameter	Analysis method	$R^2_{adj.}$; *p*-value	Model output	RMSE
Annual mean surface CO_2	Shift in the mean	0.62; $p < 0.001$	CP1: 2010 (2008–2011)	
			CP2: 2018 (2017–2020)	
	Piece-wise regr.	n.s.		
Hypolimnetic CO_2	Shift in the mean	n.s.		
	Piece-wise regr.	n.s.		
Deep hypo. CO_2	Shift in the mean	n.s.		
	Piece-wise regr.	n.s.		
CO_2 flux	Shift in the mean	0.72; $p < 0.001$	CP1: 2011 (2010–2012)	
			CP2: 2018 (2014–2019)	
	Piece-wise regr.	n.s.		
Upper layer DO	Shift in the mean	0.25; $p < 0.01$	CP: 2016 (2007–2020)	
	Piece-wise regr.	n.s.		
Hypolimnetic DO	Shift in the mean	0.39; $p < 0.001$	CP: 2007 (2002–2009)	11.6%
	Piece-wise regr.	0.57; $p < 0.05$	1995–2018: +17% DO dec^{-1}	9.7%
			2019–2022: −9% DO yr^{-1}	
Deep hypo. DO	Shift in the mean	0.33; $p < 0.01$	CP1: 2011 (2009–2012)	7.9%
			CP2: 2015 (2012–2018)	
	Piece-wise regr.	0.53; $p < 0.01$	1995–2018: +17% DO dec^{-1}	10.1%
			2019–2022: −8% DO yr^{-1}	

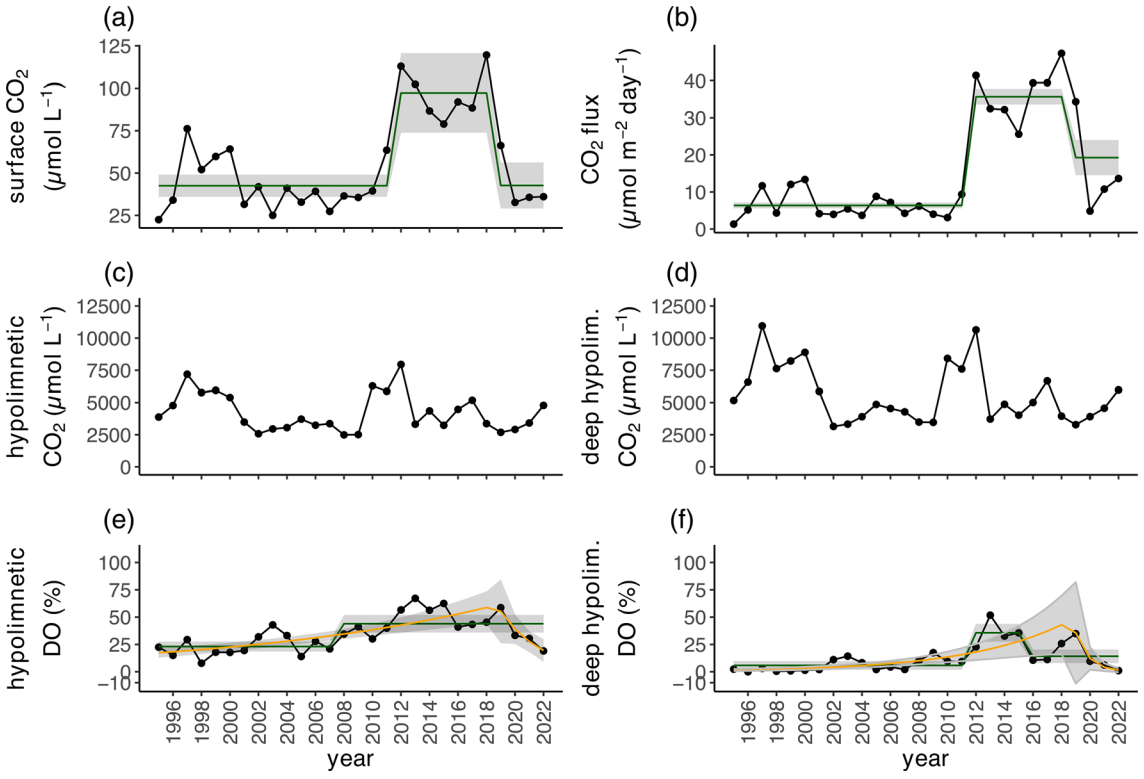

Fig. 4. Annual mean values (black points) and modeled patterns by shift in the mean analysis (green line) or piece-wise regression (orange line) for (**a**) surface CO_2 (μmol L^{-1}), (**b**) CO_2 flux (μmol CO_2 m^{-2} d^{-1}), (**c**) hypolimnetic CO_2 (μmol L^{-1}), (**d**) deep hypolimnetic CO_2 (μmol L^{-1}), (**e**) hypolimnetic DO (% saturation), and (**f**) deep hypolimnetic DO (% saturation). The gray band is the 95% confidence interval for models.

The standardized regression coefficients of hypolimnetic DO (0.22), silica (0.20), and SPI (0.16) were quite similar.

Upper layer, hypolimnetic, and deep hypolimnetic DO

Monthly data

Monthly DO of the upper layer ($mean_{1995–2022}$: 107 ± 12% DO) showed a seasonal pattern with increasing values from mid-February to July and decreasing values from August to mid-January and no trend (Supporting Information Fig. S8). Monthly hypolimnetic DO showed a seasonal pattern and a trend (Table 1; Fig. 3e), while monthly deep hypolimnetic DO only showed a trend (Table 1; Fig. 3f). The trend of hypolimnetic DO showed an increase with 2000 and 2009 and a decrease with 2018 (Table 1; Fig. 3e). Similarly, the trend of the deep hypolimnetic DO showed an increase with 2009 and a decrease with 2018 for several years (Table 1; Fig. 3f). The increasing trend starting with 2009 and the decreasing trend starting with 2018 of monthly hypolimnetic and deep hypolimnetic DO were like that of surface CO_2 concentrations (Table 1; Fig. 3a,e,f).

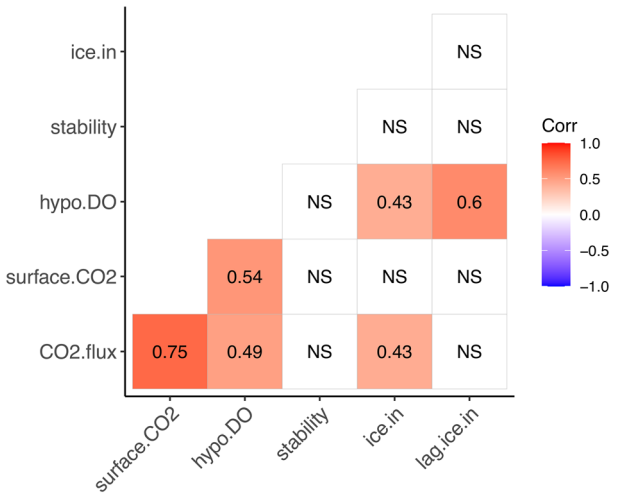

Fig. 6. Spearman correlation matrix of annual mean values of surface CO_2 (μmol L^{-1}; surface.CO2), CO_2 flux (μmol CO_2 m^{-2} d^{-1}; CO2.flux), hypolimnetic DO (% saturation; hypo.DO), Schmidt stability (J m^{-2}; stability), ice-in day of the year (ice.in), and ice-in doy of the preceding year (lag.ice.in); not statistically significant (NS).

Annual data

The annual mean of the upper layer DO showed slightly lower values ($mean_{1995–2016}$: 106 ± 5.6% DO) after the change point than before ($mean_{2017–2022}$: 112 ± 3.8% DO; Table 2).

Annual mean hypolimnetic DO showed two change points with overlapping confidence intervals, and thus only one change point was considered (Table 2; Fig. 4e). The hypolimnetic DO was lower ($mean_{1995–2006}$: 23 ± 9.5% DO;

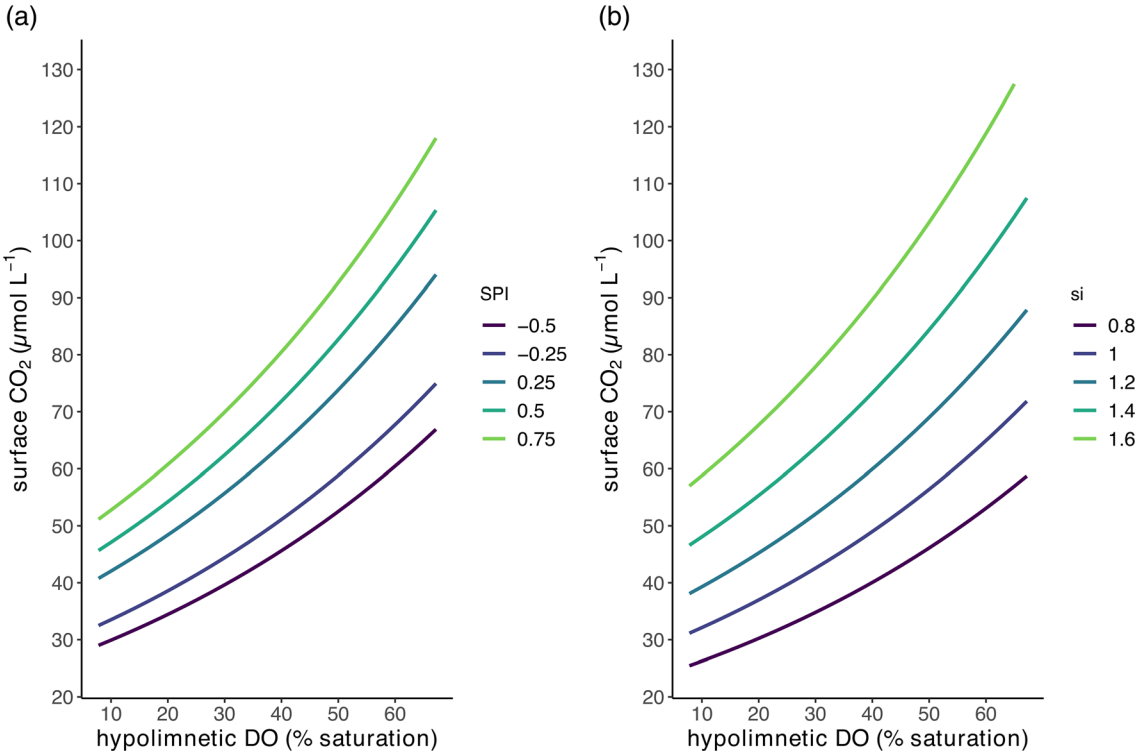

Fig. 5. Dependence of annual mean surface CO_2 concentrations (μmol L^{-1}) on annual mean hypolimnetic DO (% saturation) and on (**a**) different levels of annual mean SPI holding annual mean silica at the mean concentration (i.e., 1.13 mg SiO_2 L^{-1}); and on (**b**) different levels of silica (si; mg SiO_2 L^{-1}) holding annual mean SPI at the mean value (i.e., −0.003 SPI) as modeled by multiple linear regression.

Fig. 4e) before the change point than after ($mean_{2007–2022}$: 44 ± 13.7% DO). With piece-wise regression (Fig. 4e), annual mean hypolimnetic DO continuously increased until 2018 and then decreased (Table 2).

Annual mean deep hypolimnetic DO showed two change points delimiting a period of highest DO ($mean_{2011–2014}$ = 36 ± 12.1% DO) with lower values before ($mean_{1995–2010}$ = 6 ± 5.3% DO) and after ($mean_{2015–2022}$ = 14 ± 11.8% DO; Table 2; Fig. 4f). With piece-wise regression, annual mean deep hypolimnetic DO continuously increased until 2018 and then decreased like hypolimnetic DO (Table 2; Fig. 4f). Only with piece-wise regression the decreases in hypolimnetic and deep hypolimnetic DO occurred at the same time as the decrease in surface CO_2 and CO_2 flux.

Correlation between climate-induced mixing indices and surface CO_2 concentrations and CO_2 flux

Annual mean surface CO_2 and CO_2 flux were highly correlated between each other (Fig. 6). Hypolimnetic DO was more correlated with surface CO_2 concentrations than with CO_2 flux. As hypothesized by Flaim et al. (2020) that late ice in of the preceding year determines mixing and therefore hypolimnetic DO in the following year in Lake Tovel, hypolimnetic DO showed a higher correlation with ice-in doy of the preceding year than with ice-in doy of the same year (Fig. 6). However, surface CO_2 was not correlated with ice-in doy at all, and CO_2 flux was only correlated with ice-in doy of the same year. Schmidt stability was not correlated with any of the selected parameters.

Discussion

At the decadal scale, Lake Tovel underwent a change from meromixis to dimixis because of later ice-in that allowed for longer autumn mixing and therefore replenishment of the hypolimnetic oxygen (Flaim et al. 2020). This study showed that concomitantly to hypolimnetic oxygen also surface CO_2 concentrations and CO_2 fluxes underwent marked changes.

Driver of decadal changes in surface CO_2 concentrations

In general, climate conditions (temperature and external input) determine the dissolved inorganic carbon content of lakes (Hanson et al. 2006). Here, monthly and annual patterns of surface CO_2 concentrations were generally mirrored by hypolimnetic and deep hypolimnetic DO, indicating a close link between these parameters. Furthermore, in linear modeling, surface CO_2 increased with hypolimnetic DO, precipitation, and silica, both with monthly and annual data. Hypolimnetic DO is a proxy for deep water mixing driven by later ice-in (Flaim et al. 2020). Also here, as indicated by correlation analysis, hypolimnetic DO increased with later ice-in. Water column mixing does not only transport DO to the hypolimnion (Flaim et al. 2020), it also transports deep water CO_2 to the surface (Baehr and DeGrandpre 2004; Kuss et al. 2006; Saber et al. 2020). Silica is retained in the monimolimnion of meromictic lakes and upwelling can increase its bioavailability (Scibona et al. 2022). Thus, we suggest that hypolimnetic DO and silica are proxies for CO_2 upwelling, an internal process determining surface CO_2. Precipitation induces mixing because of heat loss (Saber et al. 2020), washes allochthonous organic material into lakes (Caldero-Pascual et al. 2022), and leads to external hydrologic input of inorganic carbon (Striegl and Michmerhuizen 1998; Stets et al. 2009). The range of total alkalinity in Lake Tovel indicates dependence on allochthonous inorganic carbon input (Marcé et al. 2015). Thus, we suggest that precipitation is a proxy for external carbon input and mixing. In summary, the modeling results and the overlap between temporal trends indicated that surface CO_2 of Lake Tovel is driven by external (loading of allochthonous carbon) and internal (lake mixing) factors at the decadal scale.

While it is impossible without a proper carbon budget to decide which factor prevails (Verheijen et al. 2022), the higher standardized regression coefficient for hypolimnetic DO than SPI, the missing trend of SPI at seasonal and annual scale as proxy for precipitation, and hypolimnetic DO mirroring surface CO_2 indicate that mixing might be more important than allochthonous carbon input for the observed trends of surface CO_2. Nevertheless, annual mean surface CO_2 was not directly correlated with ice-in, the driver of deep water mixing. Furthermore, we acknowledge that hypolimnetic DO showed the increase in 2010 with shift in the mean analysis and the 2018 decline with piece-wise regression. This might be explained by the fact that changes close to the start or end of a time-series are difficult to reveal with a shift in the mean analysis. Therefore, to finally decide on the importance of CO_2 predictors, a more detailed analysis and a longer time-series is fundamental.

Temporal changes in surface CO_2 concentrations

In Lake Tovel, surface CO_2 showed an upward shift with the year 2010 and a downward shift with the year 2018. Increased surface water temperatures lead to less mixing and intensified stratification (Woolway and Merchant 2019) and to declining surface DO in some lakes (Jane et al. 2022). In Lake Tovel, monthly surface water temperature is increasing with a minimal effect on surface DO (Flaim et al. 2020; this study). However, Flaim et al. (2020) found an increase in hypolimnetic DO linked to increased mixing from the year 2010 onwards. Similarly, we suggest that the upward shift in surface CO_2 was linked to increased DO replenishment that also led to CO_2 upwelling. We, further, suggest that as lake water warming continued, increased stratification offset the positive effect of a prolonged ice-free period from the year 2018 onwards, and thus autumn mixing decreased and surface CO_2 and CO_2 flux also decreased. Only further monitoring will show if these trends continue in Lake Tovel. Since climate warming leads to decreased CO_2 flux in other areas and lakes worldwide (Finlay et al. 2015; Brothers et al. 2021), we expect the observed trends to continue.

Schmidt stability, a classical index of water column stability and thus mixing did not explain surface CO_2 in

environmental modeling. Furthermore, annual mean Schmidt stability was not correlated with annual mean surface CO_2 and hypolimnetic DO. Flaim et al. (2020) postulated that mixing below 30 m is mainly indicated by oxygen and conductivity rather than by water density-based mixing indices such as Schmidt stability or Lake number. Similarly, water density often indicates mixing while other parameters such as pH, oxygen, or conductivity are not homogenous (Gray et al. 2020). Thus, we corroborated that other indices such as hypolimnetic DO that are not related to water density should also be considered to achieve a holistic understanding of the effect of mixing.

Link between hypolimnetic CO_2 and surface CO_2 concentrations

While hypolimnetic DO was linked to surface CO_2, hypolimnetic and deep hypolimnetic CO_2 only partly mirrored surface CO_2 concentrations at the monthly scale and not at all at the annual scale. While we reasoned that increased autumn mixing replenishes DO in the deeper layers and transports CO_2 from the deepest layer to the surface, we expected a decline in deep water CO_2. However, both hypolimnetic and the deep hypolimnetic CO_2 increased after 2010, the year of DO replenishment and increasing surface CO_2. In the Baltic Sea, re-oxygenation of the deep layers led to an increase in the mineralization rate (Hylén et al. 2021). Thus, for the 2010 increase in hypolimnetic CO_2, we speculate that DO replenishment might have boosted aerobic respiration while in other circumstances the hypolimnetic CO_2 remained unaffected by intensified mixing and DO replenishment. Since hypolimnetic temperature did not show any trend patterns, we excluded temperature effects as driver for the hypolimnetic CO_2 changes (Gudasz et al. 2010).

Seasonal changes in surface CO_2 concentrations and upper layer DO

Apart from decadal trends, seasonal changes are also important to understand carbon cycling in lakes. Here, surface CO_2 and upper layer DO showed an inverse seasonal pattern (high CO_2 and low DO during autumn and low CO_2 and high DO during summer). Also in the Baltic Sea (Kuss et al. 2006) and an oligotrophic alpine lake (Saber et al. 2020) surface CO_2 and DO show an inverse seasonal pattern. While there is a clear inverse coupling of surface CO_2 and hypolimnetic DO trends at the seasonal scale, the type of drivers of these trends may shift from biological ones during summer to abiotic ones during autumn.

Seasonal and decadal patterns of CO_2 flux

CO_2 fluxes depend on surface CO_2 concentrations and gas transfer velocity. CO_2 flux in Lake Tovel showed the same change points and trend patterns as surface CO_2, both with monthly and annual data. Therefore, both parameters were linked at a decadal scale. Furthermore, there was a seasonal mismatch between surface CO_2 (highest during autumn) and CO_2 emissions (highest after ice-out). In lakes, much CO_2 is released during spring ice break-up (Verheijen et al. 2022) while also higher CO_2 emissions are found during autumn than spring (López Bellido et al. 2009; Scholz et al. 2021). A short water residence time as driver for allochthonous inorganic carbon input increases CO_2 emissions in boreal lakes (Weyhenmeyer et al. 2015). Lake Tovel generally has a shorter water residence time in spring than during the rest of the year (Obertegger et al. 2007). Here, surface CO_2 concentrations were lower in spring than summer or autumn and gas transfer velocity was highest during spring. We suggest, therefore, that at a seasonal scale high CO_2 flux was primarily linked to high gas transfer velocity and secondly to allochthonous carbon input, determining the differences between seasons.

Generally, mountain lakes emit less CO_2 compared with other freshwater ecosystems (Cohen and Melack 2020; Ejarque et al. 2021), possibly because of low primary production and colder air and water temperature limiting metabolic processes, and/or low water residence time leading to flushing events. Furthermore, inland lakes in general (Lauerwald et al. 2023) and high-latitude lakes (Verheijen et al. 2022) show a huge variability in yearly CO_2 emissions. According to our hypothesis of low and changing CO_2 emissions in oligotrophic Lake Tovel, CO_2 emissions (range: −3–189 μmol CO_2 μmol m^{-2} d^{-1}) were much lower ($\sim$ 1000 times) than of other lakes and reservoirs (Finlay et al. 2015; Saidi and Koschorreck 2017; Golub et al. 2023) and showed periods of varying intensity.

Conclusions

Mountain lakes are sensitive to climate change (Thompson et al. 2005) but little is known on its effects on the carbon cycle. Lake Tovel can be a model system to understand the interaction of climate warming and biogeochemical processes in low-wind and ice-covered mountain lakes. Specifically, Lake Tovel transitioned between periods of high and low surface CO_2 concentrations and CO_2 emissions depending on allochthonous carbon input and on the counteracting forces of earlier ice-in favoring mixing and increased stratification inhibiting mixing. Future studies must show if this is a general pattern valid for mountain lakes more broadly. In Lake Tovel, statements on the extend of surface CO_2 concentrations and CO_2 emissions depended on the temporal period considered, and this underlines the importance of long-term data to exposit the evolution of on-going processes and ecosystems.

Data availability statement

The monthly time series data supporting this study are available from the corresponding author, U.O., upon reasonable request. Yearly mean data and exemplary analyses are deposited in Zenodo 0.5281/zenodo.10777273.

References

Abril, G., and others. 2015. Large overestimation of pCO_2 calculated from pH and alkalinity in acidic, organic-rich freshwaters. Biogeosciences **12**: 67–78. doi:10.5194/bg-12-67-2015

Bade, D. L. 2009. Gas exchange at the air-water interface. Encycl. Inland Waters **3**: 70–78.

Baehr, M. M., and M. D. DeGrandpre. 2002. Under-ice CO 2 and O 2 variability in a freshwater lake. Biogeochemistry **61**: 95–113.

Baehr, M. M., and M. D. DeGrandpre. 2004. In situ pCO_2 and O_2 measurements in a lake during turnover and stratification: Observations and modeling. Limnol. Oceanogr. **49**: 330–340. doi:10.4319/lo.2004.49.2.0330

Bates, D., M. Maechler, B. Bolker, and S. Walker. 2015. Fitting linear mixed-effects models using lme4. J. Stat. Softw. **67**: 1–48. doi:10.18637/jss.v067.i01

Brothers, S., D. Bowes, W. D. Pearse, S. Tank, R. Vanengen, and P. Sibley. 2021. Declining summertime pCO_2 in tundra lakes in a granitic landscape. Global Biogeochem. Cycles **35**: e2020GB006850. doi:10.1029/2020GB006850

Caldero-Pascual, M., and others. 2022. The importance of allochthonous organic matter quality when investigating pulse disturbance events in freshwater lakes: A mesocosm experiment. Hydrobiologia **849**: 3905–3929. doi:10.1007/s10750-021-04757-w

Carey, C. C., and others. 2022. Anoxia decreases the magnitude of the carbon, nitrogen, and phosphorus sink in freshwaters. Glob. Chang. Biol. **28**: 4861–4881.

Cellamare, M., A. M. Lancon, M. Leitão, L. Cerasino, U. Obertegger, and G. Flaim. 2016. Phytoplankton functional response to spatial and temporal differences in a cold and oligotrophic lake. Hydrobiologia **764**: 199–209. doi:10.1007/s10750-015-2313-2

Cohen, A. P., and J. M. Melack. 2020. Carbon dioxide supersaturation in high-elevation oligotrophic lakes and reservoirs in the Sierra Nevada, California. Limnol. Oceanogr **65**: 612–626.

Dugan, H. A., and others. 2016. Consequences of gas flux model choice on the interpretation of metabolic balance across 15 lakes. Inland Waters **6**: 581–592.

Ejarque, E., K. Scholz, G. Wohlfahrt, T. J. Battin, M. J. Kainz, and J. Schelker. 2021. Hydrology controls the carbon mass balance of a mountain lake in the eastern European Alps. Limnol. Oceanogr. **66**: 2110–2125.

Escoffier, N., P. Perolo, G. Many, N. T. Pasche, and M. E. Perga. 2023. Fine-scale dynamics of calcite precipitation in a large hardwater lake. Sci. Total Environ. **864**: 160699.

Finlay, K., R. J. Vogt, M. J. Bogard, B. Wissel, B. M. Tutolo, G. L. Simpson, and P. R. Leavitt. 2015. Decrease in CO_2 efflux from northern hardwater lakes with increasing atmospheric warming. Nature **519**: 215–218. doi:10.1038/nature14172

Flaim, G., A. Nishri, F. Camin, S. Corradini, and U. Obertegger. 2019. Shift from nival to pluvial recharge of an aquifer-fed lake increases water temperature. Inland Waters **9**: 261–274.

Flaim, G., D. Andreis, S. Piccolroaz, and U. Obertegger. 2020. Ice cover and extreme events determine dissolved oxygen in a placid mountain lake. Water Res. Res. **56**: e2020WR027321. doi:10.1029/2020WR027321

Golub, M., and others. 2023. Diel, seasonal, and inter-annual variation in carbon dioxide effluxes from lakes and reservoirs. Environ. Res. Lett. **18**: 34046. doi:10.1088/1748-9326/acb834

Gray, E., E. B. Mackay, J. A. Elliott, A. M. Folkard, and I. D. Jones. 2020. Wide-spread inconsistency in estimation of lake mixed depth impacts interpretation of limnological processes. Water Res. **168**: 115136. doi:10.1016/j.watres.2019.115136

Gudasz, C., D. Bastviken, K. Steger, K. Premke, S. Sobek, and L. J. Tranvik. 2010. Temperature-controlled organic carbon mineralization in lake sediments. Nature **466**: 478–483. doi:10.1038/nature09186

Hanson, P. C., S. R. Carpenter, D. E. Armstrong, E. H. Stanley, and T. K. Kratz. 2006. Lake dissolved inorganic carbon and dissolved oxygen: Changing drivers from days to decades. Ecol. Monogr. **76**: 343–363 www.jstor.org/stable/27646047

Hylén, A., S. J. van de Velde, M. Kononets, M. Luo, E. Almroth-Rosell, and P. O. Hall. 2021. Deep-water inflow event increases sedimentary phosphorus release on a multi-year scale. Biogeosciences **18**: 2981–3004. doi:10.5194/bg-18-2981-2021

Jane, S. F., J. L. Mincer, M. P. Lau, A. S. Lewis, J. T. Stetler, and K. C. Rose. 2022. Longer duration of seasonal stratification contributes to widespread increases in lake hypoxia and anoxia. Glob. Chang. Biol. **29**: 1009–1023. doi:10.1111/gcb.16525

Kratzer, G., and R. Furrer. 2022. varrank: Heuristics Tools Based on Mutual Information for Variable Ranking. R Package Version 0.5. https://CRAN.R-project.org/package=varrank

Kuhn, M. 2022. caret: Classification and Regression Training. R Package Version 6.0–93. https://CRAN.R-project.org/package=caret

Kuhn, M., and H. Wickham. 2020. Tidymodels: A collection of packages for modeling and machine learning using tidyverse principles. https://www.tidymodels.org

Kuss, J., and B. Schneider. 2004. Chemical enhancement of the CO_2 gas exchange at a smooth seawater surface. Mar. Chem. **91**: 165–174. doi:10.1016/j.marchem.2004.06.007

Kuss, J., W. Roeder, K.-P. Wlost, and M. D. DeGrandpre. 2006. Time-series of surface water CO_2 and oxygen measurements on a platform in the central Arkona Sea (Baltic Sea): Seasonality of uptake and release. Mar. Chem. **101**: 220–232. doi:10.1016/j.marchem.2006.03.004

Lauerwald, R., and others. 2023. Inland water greenhouse gas budgets for RECCAP2: 2. Regionalization and homogenization of estimates. Global Biogeochem. Cycles **37**: e2022GB007658. doi:10.1029/2022GB007658

Lenth, R. 2022. Emmeans: Estimated marginal means, aka least-squares means. R Package Version 1.8.1–1. https://CRAN.R-project.org/package=emmeans

López Bellido, J., T. Tulonen, P. Kankaala, and A. Ojala. 2009. CO_2 and CH_4 fluxes during spring and autumn mixing periods in a boreal lake (Pääjärvi, southern Finland), CO2 and CH4 fluxes during spring and autumn mixing periods in a boreal lake (Pääjärvi, southern Finland). J. Geophys. Res. Biogeosci. **114**: G04007. doi:10.1029/2009JG000923

Maetens, W. 2019. standaRdized: Standardized Index Calculation. R Package Version 1.0.

Mangiafico, S. 2017. Package 'rcompanion'. Cran Repos **20**: 1–71.

Marcé, R., B. Obrador, J.-A. Morguí, J. Lluis Riera, P. López, and J. Armengol. 2015. Carbonate weathering as a driver of CO_2 supersaturation in lakes. Nat. Geosci. **8**: 107–111. doi:10.1038/ngeo2341

Moser, K. A., and others. 2019. Mountain lakes: Eyes on global environmental change. Glob. Planet. Change **178**: 77–95.

Moss, B. 2012. Cogs in the endless machine: Lakes, climate change and nutrient cycles: A review. Sci. Tot. Environ. **434**: 130–142.

Morales-Pineda, M., A. Cózar, I. Laiz, B. Úbeda, and J. Á. Gálvez. 2014. Daily, biweekly, and seasonal temporal scales of pCO2 variability in two stratified Mediterranean reservoirs. J. Geophys. Res.: Biogeosci. **119**: 509–520. doi:10.1002/2013JG002317

Moulton, T. L. 2018. rMR: Importing Data from Loligo Systems Software, Calculating Metabolic Rates and Critical Tensions. R package version 1.1.0, https://CRAN.R-project.org/package=rMR

Muggeo, V. M. R. 2017. Interval estimation for the breakpoint in segmented regression: A smoothed score-based approach. Austr. N. Z. J. Stat. **59**: 311–322. doi:10.1111/anzs.12200

Natchimuthu, S., I. Sundgren, M. Gålfalk, L. Klemedtsson, and D. Bastviken. 2017. Spatiotemporal variability of lake pCO_2 and CO_2 fluxes in a hemiboreal catchment. J. Geophys. Res.: Biogeosci. **122**: 30–49.

Obertegger, U., G. Flaim, M. G. Braioni, R. Sommaruga, F. Corradini, and A. Borsato. 2007. Water residence time as a driving force of zooplankton structure and succession. Aquat. Sci. **69**: 575–583. doi:10.1007/s00027-007-0924-z

Parkhurst, D. L., and C. A. J. Appelo. 2013. Description of input and examples for PHREEQC version 3–a computer program for speciation, batch-reaction, one-dimensional transport, and inverse geochemical calculations. US Geological Survey Techniques and Methods, p. 497 http://pubs.usgs.gov/tm/06/a43

Pighini, S., M. Ventura, F. Miglietta, and G. Wohlfahrt. 2018. Dissolved greenhouse gas concentrations in 40 lakes in the alpine area. Aquat. Sci. **80**: 1–13.

R Core Team. 2023. R: A language and environment for statistical computing. R Foundation for Statistical Computing, https://www.R-project.org/

Read, J. S., and others. 2012. Lake-size dependency of wind shear and convection as controls on gas exchange. Geophys. Res. Lett. **39**: L09405.

Rice, E. W., R. B. Baird, A. D. Eaton, and L. S. Clesceri. 2017. Standard methods for the examination of water and wastewater, 23rd ed. American Public Health Association, American Water Works Association, Water Environment Federation.

Saber, A., D. E. James, and I. A. Hannoun. 2020. Effects of lake water level fluctuation due to drought and extreme winter precipitation on mixing and water quality of an alpine lake, case study: Lake arrowhead, California. Sci. Total Environ. **714**: 136762. doi:10.1016/j.scitotenv.2020.136762

Sadro, S., J. M. Melack, J. O. Sickman, and K. Skeen. 2019. Climate warming response of mountain lakes affected by variations in snow. Limnol. Oceanogr. Lett. **4**: 9–17. doi:10.1002/lol2.10099

Saidi, H., and M. Koschorreck. 2017. CO_2 emissions from German drinking water reservoirs estimated from routine monitoring data. Sci. Total Environ. **581–582**: 10–18. doi:10.1016/j.scitotenv.2017.01.004

Scholz, K., E. Ejarque, A. Hammerle, M. Kainz, J. Schelker, and G. Wohlfahrt. 2021. Atmospheric CO_2 exchange of a small mountain lake: Limitations of eddy covariance and boundary layer modeling methods in complex terrain. J. Geophys. Res. Biogeosci. **126**: e2021JG006286.

Scibona, A., D. Nizzoli, M. Hupfer, G. Valerio, M. Pilotti, and P. Viaroli. 2022. Decoupling of silica, nitrogen and phosphorus cycling in a meromictic subalpine lake (lake Iseo, Italy). Biogeochemistry **159**: 371–392. doi:10.1007/s10533-022-00933-9

Seekell, D. A., and C. Gudasz. 2016. Long-term pCO_2 trends in Adirondack Lakes. Geophysical Res. Lett. **43**: 5109–5115.

Simpson, G. 2023. gratia: Graceful ggplot-Based Graphics and Other Functions for GAMs Fitted using mgcv. R Package Version 0.8.1, https://gavinsimpson.github.io/gratia/

Stets, E. G., R. G. Striegl, G. R. Aiken, D. O. Rosenberry, and T. C. Winter. 2009. Hydrologic support of carbon dioxide flux revealed by whole-lake carbon budgets. J. Geophys. Res. **114**: G01008. doi:10.1029/2008JG000783

Striegl, R. G., and C. M. Michmerhuizen. 1998. Hydrologic influence on methane and carbon dioxide dynamics at two north-central Minnesota lakes. Limnol. Ocenogr. **43**: 1519–1529.

Thompson, R., C. Kamenik, and R. Schmidt. 2005. Ultrasensitive alpine lakes and climate change. J. Limnol. **64**: 139.

Toavs, T. R., C. T. Hasler, C. D. Suski, and S. R. Midway. 2023. A 30-year dataset of CO_2 in flowing freshwaters in the United States. Sci. Data Nat. **10**: 20. doi:10.1038/s41597-022-01915-0

United States Geological Survey (USGS). 2023. Hardness of water. USGS, https://www.usgs.gov/special-topics/water-science-school/science/hardness-water

Vachon, D., and P. A. Del Giorgio. 2014. Whole-lake CO_2 dynamics in response to storm events in two morphologically different lakes. Ecosystems **17**: 1338–1353.

Vachon, D., and others. 2020. Paired O2–CO2 measurements provide emergent insights into aquatic ecosystem function. Limnol. Oceanogr. Lett. **5**: 287–294.

Verheijen, H. A., M. Klaus, D. A. Seekell, and J. Karlsson. 2022. Magnitude and origin of CO_2 evasion from high-latitude lakes. J. Geophys. Res.: Biogeosci. **127**: e2021JG006768. doi:10.1029/2021JG006768

Weyhenmeyer, G. A., S. Kosten, M. B. Wallin, L. J. Tranvik, E. Jeppesen, and F. Roland. 2015. Significant fraction of CO_2 emissions from boreal lakes derived from hydrologic inorganic carbon inputs. Nat. Geosci. **8**: 933–936. doi:10.1038/ngeo2582

Wiik, E., H. A. Haig, N. M. Hayes, K. Finlay, G. L. Simpson, R. J. Vogt, and P. R. Leavitt. 2018. Generalized additive models of climatic and metabolic controls of subannual variation in pCO_2 in productive hardwater lakes. J. Geophys. Res.: Biogeosci. **123**: 1940–1959. doi:10.1029/2018JG004506

Wilson, H. L., and others. 2020. Variability in epilimnion depth estimations in lakes. Hydrol. Earth Syst. Sci. **24**: 5559–5577. doi:10.5194/hess-24-5559-2020

Winslow, L. A., J. A. Zwart, R. D. Batt, H. A. Dugan, R. I. Woolway, J. R. Corman, P. C. Hanson, and J. S. Read. 2016. LakeMetabolizer: An R package for estimating lake metabolism from free- water oxygen using diverse statistical models. Inland Waters **6**: 622–636. doi:10.1080/IW-6.4.883

Winslow, L. A., J. Read, R. Woolway, J. Brentrup, T. Leach, J. Zwart, S. Albers, and D. Collinge. 2019. rLakeAnalyzer: Lake Physics Tools. R Package Version 1.11.4.1, https://CRAN.R-project.org/package=rLakeAnalyzer

Woolway, R. I., and C. J. Merchant. 2019. Worldwide alteration of lake mixing regimes in response to climate change. Nat. Geosci. **12**: 271–276. doi:10.1038/s41561-019-0322-x

Acknowledgments

This project was funded by FEM (U.O.). We thank Ralph Tollrian for valuable comments and two anonymous referees for their constructive suggestions. Open Access funding enabled and organized by Projekt DEAL.

Conflict of Interest

None declared.

Submitted 23 September 2023
Revised 11 March 2024
Accepted 17 March 2024

Associate editor: John M. Melack